The Sequence of the Myosin 50−20K Loop Affects Myosin's Affinity for Actin throughout the Actin−Myosin ATPase Cycle and Its Maximum ATPase Activity†

Coleen T. Murphy and James A. Spudich*

Departments of Biochemistry and Developmental Biology, Stanford University School of Medicine, Stanford, California 94305

Received November 10, 1998; Revised Manuscript Received January 22, 1999

ABSTRACT: We are interested in the role that solvent-exposed, proteolytically sensitive surface loops play in myosin function. The 25−50K loop, or loop 1, is near the ATP binding site, while the 50−20K loop (loop 2) is in the actin binding site. Through chimeric studies, we have found that loop 1 affects ADP release [Murphy, C. T., and Spudich, J. A. (1998) *Biochemistry 37*, 6738−44], while loop 2 affects the actin-activated ATPase activity [Uyeda, T. Q.-P., et al. (1994) *Nature 368*, 567−9]. In the study described here, we have found that the k_{cat} of the actin-activated ATPase activity is changed by the loop 2 substitutions in a manner that reflects the relative actin-activated ATPase activities of the donor myosins. Additionally, changes in loop 2 affect the affinity of myosin for actin both in the presence and in the absence of nucleotides. Pre-steady-state studies together with the ATPase and affinity data suggest that while loop 2 does not affect interactions between myosin and nucleotide, it plays a role in determining the affinity of myosin for actin in various nucleotide states and in the rate-limiting transition allowing phosphate release.

Myosins use the energy of ATP binding, hydrolysis, and product release in coordination with actin binding and translocation to function as molecular motors. The details of the mechanism are becoming clearer as a result of the combination of genetic, structural, and biochemical analyses from many labs, including a large body of work describing the kinetics of the cycle (*1*−*3*). Scheme 1 describes the cycle, with two-step binding reactions simplified to one step.

Scheme 1

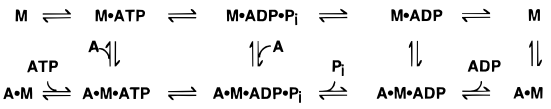

Myosin binds very tightly to actin in the absence of nucleotide, but is only weakly bound upon binding ATP (*2*); the ATP is hydrolyzed by myosin while in this weakly bound state. In the absence of actin, product release is very slow and is the rate-limiting step of the ATPase cycle (*2*). P_i[1] is induced to dissociate upon reassociation of actin in a strongly bound state; it is thought that the force-generating stroke occurs following P_i release (reviewed in refs *4*−*6*). This is immediately followed by ADP release, which allows ATP to bind and dissociate the myosin from the actin. In the presence of actin, a conformational change, possibly involving the weak-to-strong actin-binding transition, is rate-limiting for the cycle rather than the P_i release step itself (*3*).

Conventional myosin, or myosin II, is composed of a globular catalytic head domain containing both the nucleotide and actin binding sites, a light-chain binding neck that appears to act as a lever arm in producing an approximately 10 nm step, and a long coiled-coil tail that allows formation of bipolar thick filaments. Proteolysis of skeletal myosin at solvent-exposed, flexible loops cleaves the head into segments of 25, 50, and 20 kDa (*7*); the loops connecting these segments (the 25−50K and 50−20K loops, or loops 1 and 2, respectively) were not well-resolved in the crystal structures of the chicken skeletal myosin II subfragment 1 (S1) (*8*) or *Dictyostelium* S1 (*9*), indicating that they may adopt multiple conformations. While the rest of the myosin II head is well-conserved evolutionarily [60−80% identical (*10*)], the loops vary considerably both in length and in sequence (*11*).

Uyeda et al. (*12*) showed that loop 2 affects the actin-activated ATPase activity of *Dictyostelium* myosin. This was not entirely surprising, as the loop had been shown previously to be part of the actin-binding site (*7*); additionally, it was known that proteolysis of loop 2 causes decreases in the actin-activated ATPase activity (*7*, *13*, *14*). However, it was unexpected that the substitution of loop 2 from various myosins for the *Dictyostelium* loop 2 could cause an increase in the actin-activated ATPase activity, or that the activities of the chimeras would reflect the order of activities of the donor myosins. These results suggested that the sequence variability of the loops might help to fine-tune the activity of each myosin isoform (*15*).

Uyeda et al. did not determine the effect of the loop 2 changes upon k_{cat} or K_m, as assays were carried out only at subsaturating actin concentrations. There has been some

† This work was supported by NIH Grant AR42895 to J.A.S.; C.T.M. is a Howard Hughes Medical Institute Predoctoral Fellow.

* To whom correspondence should be addressed: Department of Biochemistry, SUMC, Stanford, CA 94305. Phone: (650) 723-7634. Fax: (650) 725-6044. E-mail: jspudich@cmgm.stanford.edu.

[1] Abbreviations: S1, subfragment 1; P_i, inorganic phosphate; kb, kilobase; mant, 2′(3′)-*O*-(*N*-methylanthraniloyl); BDM, 2,3-butanedione 2-monoxime; ATPγS, adenosine 5′-*O*-(3-thiotriphosphate).

10.1021/bi9826815 CCC: $18.00
Published on Web 03/05/1999

debate about whether loop 2 causes a change in k_{cat} or exerts its effects simply through changes in K_m (*16*, *17*). To more fully understand the function of the loop 2 sequences, we created the S1 forms of the two full-length *Dictyostelium* myosin chimeras with the most extreme actin-activated ATPase activities and examined their kinetics. We carried out ATPase assays over a range of actin concentrations to determine the k_{cat} and K_m, determined the affinity of the S1 chimeras for actin in various nucleotide states, and studied the pre-steady-state kinetics of individual steps of the actin−myosin cycle. Our work indicates that loop 2 plays a role in the initial interaction with actin, helps change myosin's affinity for actin during changes in its nucleotide state, and aids the transition from the weakly to strongly bound form, stimulating phosphate release. Further, it appears that these changes in activity are not due simply to changes in the net charge, but rather are caused by changes in the amino acid sequence of the loop.

MATERIALS AND METHODS

Reagents. All reagents were from Sigma (St. Louis, MO). ATPγS was found to contain 30% ADP when analyzed by HPLC; the ADP was degraded to adenosine and phosphate by purified alkaline phosphatase (a gift from P. O'Brien). The remaining ATPγS was separated from the alkaline phosphatase by centrifugation in a Centricon 30 microconcentrator (Amicon, Beverly, MA). All nucleotide experiments were carried out in buffers containing Mg^{2+} in excess of nucleotide.

Plasmid Construction. Standard methods were used for all DNA manipulations, and all restriction enzymes were from New England BioLabs (Beverly, MA). To create the S1 loop constructs, the pTIKLmyosin loop vectors were digested with *Bst*XI and *Nco*I, and these 0.7 kb fragments were purified and ligated with the pTIKL-OE-S1-His_6 vector (a gift from T. Q.-P. Uyeda) which had been partially digested with *Nco*I followed by digestion with *Bst*XI.

Dictyostelium Manipulations. All cells were grown at 22 °C in HL5 medium with 17% FM medium (Gibco BRL, Gaithersburg, MD), 100 units/mL penicillin, and 100 μg/mL streptomycin. Plasmids were electroporated into HS1, a myosin II null strain (*18*), and after initial characterization, AX3-ORF^+ cells were transformed with the same plasmids (*19*). Transformants were selected for and maintained with 5 μg/mL G418 (Gibco BRL). S1-transformed myosin null cells were grown on 530 cm^2 Petri dishes (Nalge Nunc, Naperville, IL), while transformed AX3-ORF^+ cells were grown in suspension.

Protein Purification. S1 proteins (M_r = 125 kDa) were purified as previously described (*20*, *21*). The concentration was determined spectrophotometrically at 280 nm using an extinction coefficient of 0.8 cm^2/mg. All assays were carried out on at least two preparations of myosin or S1, and in most cases more than four times, and are reported as an average of the values with standard deviations.

Actin was prepared according to the protocol of Pardee and Spudich (*22*). Actin was labeled with *N*-(1-pyrene)-iodoacetamide (Molecular Probes, Eugene, OR) as previously described (*23*). Phalloidin (Sigma) was added at a 1.5:1 molar excess to actin to stabilize the filaments for all stopped-flow and spectrophotometry experiments.

ATPase Assays. Myosin ATPase activities at 30 °C were determined by measuring the rate of release of labeled P_i using [γ-^{32}P]ATP in a TLC assay as described by Giese and Spudich (*21*). Reaction mixtures contained 25 mM imidazole (pH 7.4), 25 mM KCl, 4 mM $MgCl_2$, 1 mM DTT, 3 mM ATP, and 0.05 or 0.1 mg/mL S1. Curves were fit to the Michaelis−Menten equation in KaleidaGraph (Abelbeck Software).

Cosedimentation Assays. As described by Giese and Spudich (*21*), 1.5−21 μM S1 was centrifuged at 20 °C with 3 μM phalloidin-stabilized actin at 200000*g* in a Beckman TL-100 centrifuge (Palo Alto, CA) in the presence of 3 mM ATP in ATPase buffer (see above). Pellets were resuspended and submitted to SDS−PAGE, and the Coomassie Blue-stained gels were analyzed with the AlphaImager 2000 system (AlphaInnotech Corp., San Leandro, CA). Densities were normalized according to a standard curve and the known concentration of actin in each lane, and then were used to determine the K_d by curve fitting in KaleidaGraph (see the K_d equation below, modified for fitting $[S1]_{bound}$/[actin] vs $[S1]_{initial}$).

Fluorimetry Assays. The fluorescence of 100 nM phalloidin-stabilized pyrene actin at 20 °C in 25 mM HEPES (pH 7.4), 25 mM KCl, 10 mM $MgCl_2$, and 1 mM DTT was titrated with S1 until maximally quenched to determine the K_d of S1 for actin (*21*); experiments were carried out on a Series 2 Luminescence Spectrometer (SLM-Aminco, Rochester, NY). Affinities were also determined in the presence of 3 mM ADP, ADP and P_i, and ATPγS. In the case of ATPγS, the titration was carried out with 250 nM pyrene actin. The ADP and P_i assay was carried out in 25 mM HEPES, 25 mM potassium phosphate (pH 7.4), and 10 mM $MgCl_2$ with 3 mM ADP, both with and without 2,3-butanedione 2-monoxime (BDM, Sigma), to stabilize the ADP·P_i complex (*24*). Nucleotides were preincubated with S1, and the nucleotide was present in the pyrene actin sample as well. The excitation and emission wavelengths were 365 and 407 nm, respectively, with bandwidths of 8 and 16 nm.

Because $K_d = ([A][M])/[A{\cdot}M]$, $[A] = [A]_0 - [A{\cdot}M]$, and $[M] = [M]_0 - [A{\cdot}M]$, the following quadratic equation may be used to solve for [A·M]:

$$[A{\cdot}M] = \frac{([M]_0 + [A]_0 + K_d) \pm [([M]_0 + [A]_0 + K_d)^2 - 4([A]_0[M]_0)]^{0.5}}{2} \quad (1)$$

The fractional fluorescence (*37*) $\alpha = (F_0 - F)/(F_0 - F_\infty)$, where F_0 is the initial fluorescence, F is the observed fluorescence, and F_∞ is the final fluorescence.

Because $[A{\cdot}M] = \alpha[A]_0$, we may solve for K_d using the observed, initial, and final fluorescence and the known actin and myosin concentrations. Data were fit to the equation

$$F = F_0 - \{(F_0 - F_\infty)\{(A_t + S_t + K_d) - [(A_t + S_t + K_d)^2 - 4A_tS_t]^{0.5}\}(2A_t)^{-1}\} \quad (2)$$

where A_t and S_t are the concentrations of actin and S1, respectively, solving for K_d and F_∞; A_t was adjusted for dilution throughout the curve by adjusting A_t:

$$A_t = ([\text{actin}]_0 \times 125)/\text{Vol}_t \quad (3)$$

where $[actin]_0$ is the starting pyrene actin concentration, 125 μL is the starting volume, and Vol_t is the total volume for each titration point.

K_{II} Determinations. According to McKillop et al. (*24*),

$$K_{II} = \frac{F_0 - F_L}{F_L - F_\infty} \quad (4)$$

where F_0 is the initial fluorescence of pyrene actin (100%), F_L is the fluorescence in the presence of S1 and ligand (nucleotide), and F_∞ is the final fluorescence after addition of S1 in the absence of nucleotide (*24*), assuming little dissociation of actin to the A and M(·N) state, as was previously shown by Geeves and Jeffries (*37*). It should be noted that the K_{II} values may be skewed if a large fraction is dissociated from actin rather than weakly bound, as was assumed for the calculations.

Stopped-Flow Spectrophotometry. Stopped-flow experiments were performed at 20 °C with a DX.17MV sequential stopped-flow spectrophotometer (Applied Photophysics, Leatherhead, U.K.). Light was provided by a Hamamatsu mercury−xenon lamp (Middlesex, NJ) or an Osram Xenon lamp (Montgomery, NY) and passed through an Applied Photophysics SpectraKinetic monochromator. Pyrene actin was excited at 365 nm, and emission was monitored at 90° through a KV 380 nm cutoff filter. Nucleotide binding and release reactions were followed by measurement of 2′(3′)-*O*-(*N*-methylanthraniloyl) nucleotide fluorescence excited at 290 nm and monitored through a KV 380 nm filter. Light scattering experiments were carried out by exciting at 340 nm and monitoring at 90° through a WG 335 nm cutoff filter. Intrinsic fluorescence experiments were performed by exciting at 290 nm and monitoring through a WG320 filter. Data were analyzed by a least-squares fitting procedure (Kaleidagraph). Assays were carried out in a standard buffer of 25 mM HEPES (pH 7.4), 1 mM DTT, 5 mM $MgCl_2$, and 25 mM KCl.

To determine the off-rate of mantADP, 1 μM S1 was premixed with 5 μM mantADP, and then the complex was rapidly mixed in the stopped-flow instrument with Mg^{2+}-ATP (15 and 25 mM); the decrease in mant fluorescence was monitored. To determine the mantATP second-order binding constant, 0.5 μM S1 (final) was rapidly mixed with 5−25 μM mantATP (final concentrations) and the single-exponential rise in fluorescence was plotted against mantATP concentration. The extent of ATP binding was monitored via intrinsic fluorescence change (*25*), and the maximum rate of fluorescence change ($k_3 + k_{-3}$, the rate of hydrolysis; see Scheme 2) was measured at 5 and 25 mM Mg^{2+}ATP (final concentrations).

Scheme 2

$$M + ATP \underset{k_{-1}}{\overset{k_1}{\rightleftharpoons}} M{\bullet}ATP \underset{k_{-2}}{\overset{k_2}{\rightleftharpoons}} M^*{\bullet}ATP \underset{k_{-3}}{\overset{k_3}{\rightleftharpoons}} M^{**}{\bullet}ADP{\bullet}P_i$$

Stopped-flow determination of the affinity of S1 for actin in the absence of nucleotide was carried out according to the method of Kurzawa and Geeves (*26*) with 15 nM phalloidin-stabilized pyrene actin and 10 μM ATP, and in 20 mM MOPS (pH 7.0) and 5 mM $MgCl_2$ with 100 mM KCl. Five consecutive traces were averaged for each concentration of S1 used (10−500 nM), and the amplitude (ΔF) was plotted as a function of S1 concentration; $\Delta F = (F_{A^*} - F_{A^*M})[A^*M]$. The curve was then fit to the quadratic equation shown above (eq 2) to determine the K_d.

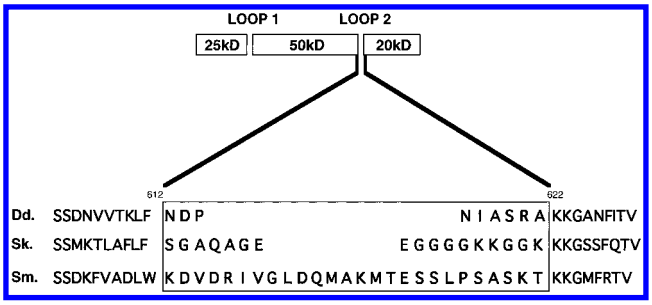

FIGURE 1: Loop 2 sequences. The *Dictyostelium* loop 2 sequence was replaced by the rabbit skeletal and chicken smooth loop 2 sequences (*12*), and the S1 form was expressed and purified as described in the text. Native skeletal muscle myosin displays high actin-activated ATPase activity [20 s^{-1} (*44*)] compared with *Dictyostelium* myosin [2−4 s^{-1} (*21*, *45*)], while the smooth muscle myosin ATPase activity is low [0.95 s^{-1} (*46*)].

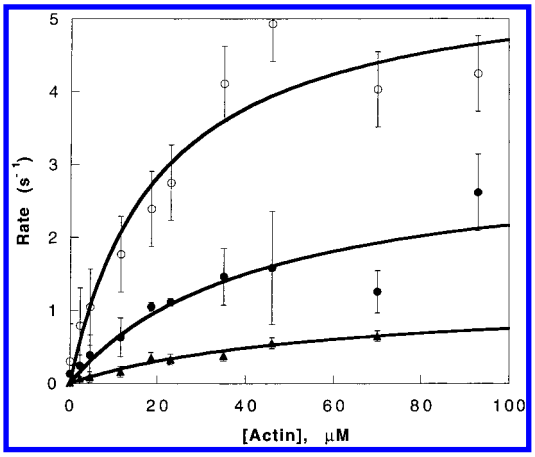

FIGURE 2: Actin-activated ATPase activities of the loop 2 chimeras. Fits to the Michaelis−Menten equation show that the skeletal chimera (○) has a higher maximal activity (5.7 ± 0.7 s^{-1}) than the wild type (●) (2.4 ± 0.6 s^{-1}) or the smooth muscle chimera (▲) (1.2 ± 0.2 s^{-1}). K_m = 43 ± 24, 20 ± 7, and 60 ± 19 μM for the wild type, skeletal chimera, and smooth chimera, respectively.

RESULTS

Role of Loop 2 in the Dictyostelium S1 Actin-Activated ATPase Cycle

Loop 2 Substitutions Change the k_{cat} of Actin-Activated ATPase Activity. Because myosin forms filaments in low salt and deviates from Michaelis−Menten behavior under these conditions (*27*), the soluble myosin head fragment S1 was used in this work. We constructed the *Dictyostelium* S1 forms of the skeletal and smooth muscle myosin chimeras (Figure 1) and measured the activities of the chimeric and wild-type S1s as a function of actin concentration. The wild-type *Dictystelium* S1 has a k_{cat} of 3.1 ± 0.8 s^{-1}; the skeletal chimera's k_{cat} was 5.7 ± 0.7 s^{-1}, and the smooth muscle chimera had a maximal activity of only 1.2 ± 0.2 s^{-1} (Figure 2 and Table 1). The basal activities were somewhat affected, with rates of 0.1 ± 0.06, 0.2 ± 0.1, and 0.04 ± 0.05 s^{-1} for the wild type, the skeletal chimera, and the smooth chimera, respectively. The skeletal chimera's K_m value was about half of that of the wild type, while the smooth chimera's K_m was increased by 50%; however, the error of these values is

Table 1: Actin-Activated S1 ATPase Data

	wild-type *Dictyostelium* S1	skeletal chimera	smooth chimera
basal ATPase (s^{-1})	0.1 ± 0.06	0.2 ± 0.1	0.04 ± 0.05
k_{cat} (s^{-1})	3.1 ± 0.8	5.7 ± 0.7	1.2 ± 0.2
K_m (μM)	43 ± 24	20 ± 7	60 ± 19
$k_{cat}/K_m \times 10^{-4}$ (M^{-1} s^{-1})	7.2 ± 3	28 ± 10	2 ± 1

Table 2: S1 Interactions with Nucleotide

	wild-type *Dictyostelium* S1	skeletal chimera	smooth chimera
ATP hydrolysis (s^{-1}) ($k_3 + k_{-3}$)	16 ± 2	13 ± 2	15 ± 4
mantADP dissociation (s^{-1})	2.5 ± 0.1	2.4 ± 0.3	2.2 ± 0.3
mantATP association (M^{-1} s^{-1}) $\times 10^{-5}$	7 ± 2	10 ± 1	9 ± 1

substantial. Nonetheless, k_{cat}/K_m was significantly affected by the loop 2 changes, with a 14-fold difference between the two chimeras (Table 1).

Loop 2 Does Not Affect Interactions between Myosin and Nucleotide. While the changes in the sequence of loop 2 substantially affect the actin-activated ATPase activity, there were no noticeable effects upon the interactions between S1 and nucleotides. The rates of nucleotide binding, release, and hydrolysis were unaffected by changes in the loop 2 sequence (Table 2). While we cannot rule out the possibility that both k_3 and k_{-3} have changed, because the change in intrinsic fluorescence due to hydrolysis measures $k_3 + k_{-3}$ rather than the separate forward and reverse rates, it seems unlikely that in each case this would result in the same measured rate unless hydrolysis were unchanged by changes in the loop 2 sequence.

Role of Loop 2 in Determining the Affinity of S1 for Actin

The Loop 2 Sequence Affects the Weak and Strong Binding Affinities. Because changing the loop 2 sequence appeared to affect the K_m for actin, we examined by other approaches the effects of changing loop 2 on the affinity of the actin−S1 interaction in various nucleotide states. We tested the weak binding affinity of each S1 for actin by cosedimenting 1.5 to 21 μM S1 with 3 μM actin in the presence of 3 mM ATP (Figure 3). (Actin concentrations below 3 μM yielded similar but less reproducible S1 sedimentation results, probably due to the lower amount of actin pelleted and Coomassie stained; higher actin concentrations would have precluded the measurement of greater affinities.) The skeletal chimera showed the strongest affinity ($K_d = 3$ μM) compared with wild-type S1 (15 μM) and the smooth chimera (21 μM). While the relative order of the K_ds agrees with the order of K_ms, the values are not identical, reflecting the fact that the two experiments measure different and multiple enzyme-bound species (*28*). ATP was added immediately before centrifuging the samples, and ATP is in a 100−1000-fold excess over enzyme; however, the sedimenting complex is most likely a mixture of A·S1·ATP and A·S1·ADP·P_i during the course of the experiment, which complicates the interpretation of the affinity constant measured in this assay.

As pointed out by Kurzawa and Geeves (*26*), to assess high-affinity interactions of S1 with actin, for example, in the absence of nucleotide, it is necessary to use low actin

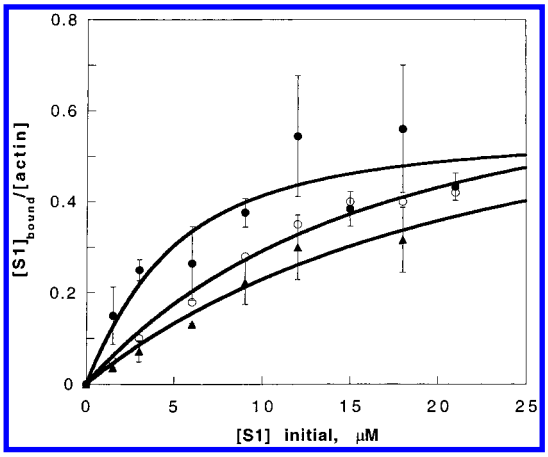

FIGURE 3: Cosedimentation assays of loop 2 chimeras with actin in the presence of 3 mM ATP. Actin (3 μM) was centrifuged with 1.5−21 μM S1 in the presence of 3 mM ATP, and the pellets were submitted to SDS−PAGE and analyzed as described in Materials and Methods. The skeletal chimera (●) shows a 5-fold higher affinity than the wild type (○) and a 7-fold higher affinity for actin than does the smooth chimera (▲): 3, 15, and 21 μM, respectively.

concentrations. We have found that actin−S1 affinities in the presence of nucleotide may also be tight enough that low actin concentrations (lower than is practical in cosedimentation assays) are necessary for their proper determinations. To determine the actin−S1 affinities in various nucleotide states, we quenched pyrene actin fluorescence by titrating with S1 in the absence of nucleotide and in the presence of ATPγS, ADP and P_i (with or without BDM), and ADP. [The K_m for ATP is 32 μM (*21*), and the K_d of actin−S1 for ADP is near 40 μM (*25*); thus, 3 mM nucleotide was assumed to be sufficient for binding.] In all cases, the order of affinities is maintained (skeletal chimera affinity > wild type > smooth chimera), while the affinities increase from low micromolar to low nanomolar as the nucleotides mimic progressive states of hydrolysis and product release (Figure 4a−d and Table 3). In the case of ADP and P_i, there was no significant difference in the presence of BDM, which has been shown to stabilize the A·M·ADP·P_i state of skeletal myosin (*24*, *29*−*31*). The K_ds and final fluorescence values of the ADP and P_i experiment are significantly different from those for the ADP and ATPγS experiments. In each case, the affinity is affected by the sequence of loop 2, with differences of 3−8-fold between the constructs. Furthermore, the final quenched fluorescence (F_∞) varied not only with nucleotide but also with chimera (Table 3); the skeletal chimera always quenched fluorescence to a greater degree than did the wild type or the smooth chimera. These differences in quenching may be due to differences in the local environment of the pyrene due to the loop sequence changes.

The concentration of pyrene actin used in these experiments (100 nM) was chosen to allow accurate determinations of the K_d down to 100 nM, but is a practical lower limit due to weak signal at lower concentrations [that is, K_d values measured at 20 and 50 nM were similar to the 100 nM results, but the final fluorescence (F_∞) was more variable]. In the absence of nucleotide, the affinity of S1 for actin is so great ($\ll$100 nM) that the measured K_d may only be an upper estimate. Nevertheless, the values we have obtained agree well with independently derived estimates (*17*) and with values derived with an alternative stopped-flow method

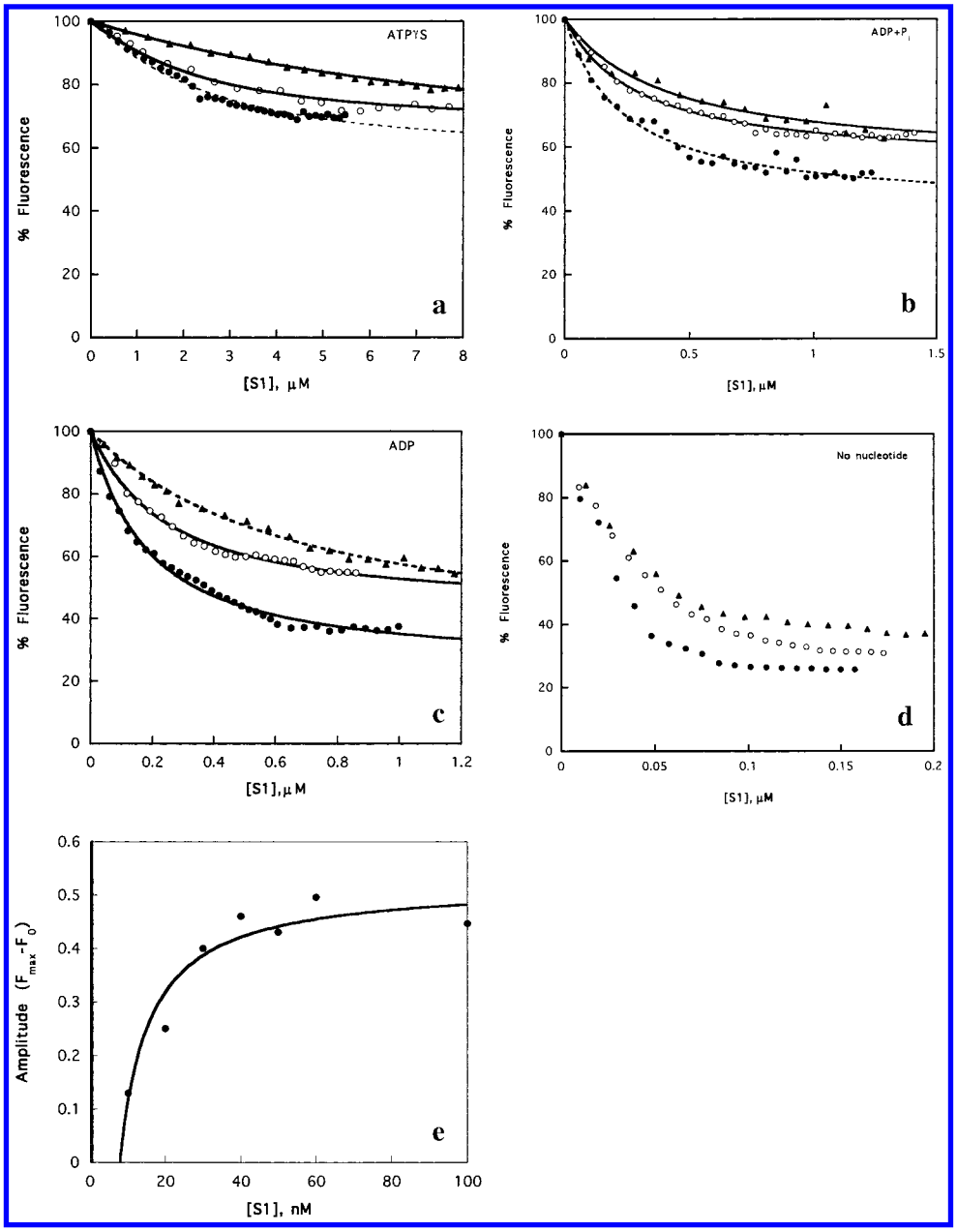

FIGURE 4: Pyrene actin titrations. The fluorescence of pyrene actin (100 nM unless otherwise noted) was quenched by the titration of S1. The skeletal chimera (●) binds more tightly to pyrene actin than does the wild type (○) or the smooth chimera (▲) in all cases, but the affinity ranges are affected by the particular nucleotide bound: (a) ATPγS (250 nM pyrene actin was used in the ATPγS experiment), (b) 3 mM ADP and 25 mM P_i, (c) 3 mM ADP, and (d) no nucleotide. No curve is shown because the affinities are significantly tighter than the pyrene actin concentration used for the experiment (see the text). (e) Stopped-flow method of pyrene actin K_d determination with 15 nM pyrene actin. Shown are the amplitudes for the skeletal chimera in 100 mM KCl; the calculated $K_d = 0.3$ nM.

developed by Kurzawa and Geeves that uses lower pyrene actin concentrations (*26*). For comparison, we used this method in the absence of nucleotide and with 15 nM pyrene actin (a practical lower limit for this assay) and found that the results agree with our fluorimetry determinations (Table 3 and Figure 4e). Phalloidin-stabilized pyrene actin (15 nM) was mixed with increasing concentrations of S1 and then rapidly mixed in the stopped-flow apparatus with 10 μM ATP. The pyrene actin dissociated from the S1 at a constant rate of 9 s^{-1}, but the amplitude increased with S1 concentration due to the increased degree of formation of quenched pyrene actin−S1; the amplitude was plotted as a function of S1 concentration and fitted to a quadratic equation (see Materials and Methods) to solve for K_d. At 100 mM KCl, the skeletal chimera's affinity was calculated to be 0.3 ± 0.2 nM, which is comparable to the fluorimetry-determined value of 0.7 nM. Thus, it appears that the low K_d values which we have determined using the fluorimetry assay are reasonable despite the fact that they were measured at 100 nM pyrene actin.

Loop 2 Affects the Attached to Rigor Transition. Geeves et al. (*35*, *36*) have proposed a three-state model for actin binding:

Scheme 3

$$\mathrm{A + M(\bullet N)} \overset{K_0}{\rightleftharpoons} \underset{\text{collision complex}}{\mathrm{A\text{ -- }M(\bullet N)}} \overset{K_I}{\rightleftharpoons} \underset{\text{A state}}{\mathrm{A\text{-}M(\bullet N)}} \overset{K_{II}}{\rightleftharpoons} \underset{\text{R state}}{\mathrm{A\bullet M\bullet (N)}}$$

where A is actin, M is myosin or S1, and N is nucleotide. In

Table 3: Actin Affinity Data

	wild-type *Dictyostelium* S1	skeletal chimera	smooth chimera
no nucleotide			
K_d (nM)	1.8 ± 2.7	0.7 ± 2.3	2.7 ± 1
F_∞ (%)	27 ± 4.7	19 ± 6.6	36 ± 1.1
ADP			
K_d (nM)	220 ± 16	170 ± 8.7	660 ± 35
F_∞ (%)	48 ± 1.4	36 ± 4	54 ± 5
K_{II}	2.6	3.8	2.6
ADP·P_i			
K_d (nM)	290 ± 17	230 ± 20	810 ± 130
F_∞ (%)	54 ± 0.8	41 ± 1.4	60 ± 4.8
K_{II}	1.7	2.7	1.7
ATPγS			
K_d (μM)	5.7 ± 0.2	1.6 ± 0.2	9 ± 1.3
F_∞ (%)	70 ± 4	66 ± 1.4	76 ± 4
K_{II}	0.7	0.72	0.6

this model, the first step (K_0) is dependent upon ionic strength, the myosin isomerization to the A ("attached") state (K_I) involves hydrophobic interactions, and the final A-to-R ("rigor", referring to the very high-affinity actin state) transition, known as K_{II}, involves both ionic and hydrophobic interactions (*35*). This model is based upon solution studies that do not address the issue of force- versus non-force-bearing states (*31*), which may add additional states to the model. We used the percentage of fluorescence in the presence and absence of ligand (ADP or ADP·P_i) to estimate values of K_{II} (Table 3). Estimates of this equilibrium indicate that the sequence of loop 2 affects not only the initial on-rate (K_0k_1, or in the case of M·ADP·P_i, the k_{cat}/K_m of the ATPase assay) but also the A-to-R transition.

Loop 2 Affects the Rate of Actin−S1 Dissociation by ATP. When a preformed complex of S1 and actin is mixed with a high concentration of Mg^{2+}ATP (10 and 25 mM final concentrations), the ATP binds to the S1 quickly [$k_{on} = 1 \times 10^5$ M^{-1} s^{-1}; the rate is estimated to be 1000 and 2500 s^{-1}, respectively, for these ATP concentrations (*25*, *32*)] and the actin subsequently dissociates from the A·S1·ATP complex: Scheme 4

$$\text{A•S1 + ATP} \rightleftharpoons \text{A•S1•ATP} \rightleftharpoons \text{A + S1•ATP}$$

The smooth muscle chimera dissociates from actin at a rate of 200 s^{-1} (Figure 5), faster than the wild type (120 s^{-1}) or the skeletal chimera (40 s^{-1}). This correlates with the weaker affinity for actin which the smooth muscle chimera displays (see Figure 3) compared to those of the wild type and the skeletal chimera.

DISCUSSION

The finding that the k_{cat} of the actin-activated ATPase activity is affected by the sequence of loop 2 was somewhat surprising because it suggests that the loop participates in the rate-limiting conformational change allowing phosphate release, presumably after actin binding, rather than simply changing the affinity for actin. A change in affinity (K_m), as reported by Rovner et al. (*16*), would seem to be a simpler explanation for the role of loop 2. However, mutagenic studies of actin showed previously that changes in the N-terminus of actin, which is postulated to interact with loop 2, can either inhibit (*33*) or stimulate (*34*) the k_{cat}, but do not affect the K_m. Additionally, Furch et al. (*17*) observed

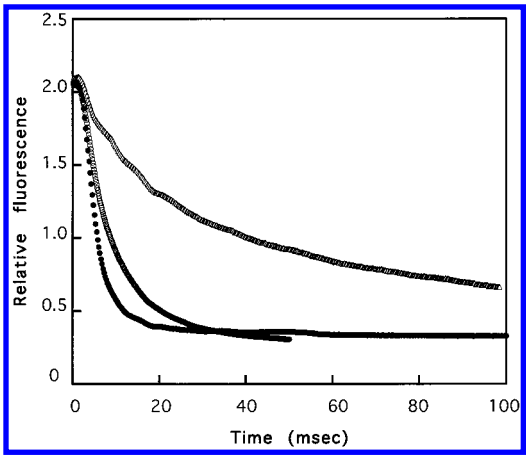

FIGURE 5: Actin−S1 dissociation by ATP. When a complex of phalloidin-stabilized actin and S1 is mixed with 20 or 50 mM ATP (10 or 25 mM final concentration), the actin dissociates from the skeletal chimera (△, upper trace) at 40 ± 5 s^{-1}, from the wild type (○, middle trace) at 120 ± 20 s^{-1}, and from the smooth chimera (●, lower trace) at 200 ± 50 s^{-1}.

an increase in the k_{cat} of the actin-activated ATPase activity when many additional charges were added to the *Dictyostelium* myosin II loop 2. The fact that the k_{cat} increased in the case of the skeletal chimera indicates that there has been a change in the rate of the rate-limiting step rather than a change in which step is rate-limiting, as might have been inferred if we had only seen decreases in the k_{cat}. Thus, the loop may be participating in a transition between two actin-bound states prior to phosphate release which is rate-limiting for the actin−myosin ATPase cycle.

The transition between an attached state and the rigor state of skeletal myosin has been described in detail by Geeves et al. Because K_0 and K_{II} (Scheme 3) are dependent upon ionic strength, Furch et al. reasoned that the addition of charged residues to loop 2 should affect these equilibria, and we used our fluorescence data to estimate K_{II} for each chimera with various nucleotides bound. While the smooth and wild-type constructs have similar K_{II} values, the skeletal construct shows a 1.5-fold increase in K_{II} in the ADP and ADP·P_i states relative to that of the wild type. While the differences between the various K_{II}s are not large, the order of the values (skeletal chimera > wild type ≥ smooth chimera) is maintained. In general, the differences in K_{II} are not as great as those observed for skeletal myosin, indicating a smaller change in free energy of the nucleotide states of *Dictyostelium* myosin, but some of these differences do seem to be mediated by loop 2.

Loop 2 does not appear to affect interactions between nucleotide and S1; specifically, nucleotide binding, hydrolysis, and release are unchanged by differences in the loop (Table 2). However, it should be noted that the rate of actin−S1 dissociation by ATP is sufficiently slowed in the case of the skeletal chimera to account for the slower motility of the full-length myosin in the work of Uyeda et al. (*12*). It has been shown previously that motility and ATPase activity are unrelated (*39*, *40*); this is due to the fact that these activities have different rate-limiting steps (*2*, *41*). Studies of loop 1, which lies near the ATP pocket, have shown that ADP release is specifically affected by changes in this loop, while other activities are completely unaffected (*32*) or less affected (*42*, *43*). Loop 2 seems to function in a similarly

specific fashion (ref *17* and this work). One possibility is that the two loops have varied to optimize activity; that is, by varying the sequence at key sites outside the core of the enzyme, one may fine-tune the activity of the particular myosin for its cellular role. Goodson et al. have proposed that the two loops have evolved at a similar rate, but these evolutionary rates vary from the rate of change of the rest of the myosin head, to achieve changes optimal for a particular myosin activity (*11*). They have also shown that the loops are actually well-conserved when myosins of like kinetic activities are compared. In fact, the two loops may co-vary to maintain the fraction of the ATPase cycle in which the myosin is strongly bound to actin, known as the duty ratio.

It should be noted that while much of our study agrees with the findings of Furch et al., the activities of our chimeras do not seem to display the same charge dependence shown by their synthetic loop constructs. Specifically, there is only an overall difference of +1 in the sequence of the skeletal chimera from the *Dictyostelium* or smooth muscle loops, yet there are large differences in activities and affinities between the chimeras; the skeletal loop chimera exhibits actin-activated ATPase activity at 20 μM actin which is 6 times greater than the activity of the synthetic loop construct with a +1 charge. The skeletal chimera also shows a greater effect upon the no-nucleotide K_d than does the +1 construct. Furthermore, there are significant differences in activities between wild-type S1 and the smooth muscle chimera S1 despite the lack of a difference in net charge of these loops. As Furch et al. noted, the natural loop sequences have an asymmetric distribution of charge which may be situated ideally to interact with negative charges on actin. Therefore, we conclude that while charges may help to generally determine some activities, the sequence of the loops, and therefore the spatial location of the residues on the actin binding face, is extremely important in determining myosin activity and actin affinity.

It is possible that while loop 2 does affect actin activation of myosin in multiple systems, its role may be different depending on the exact mechanism of the rate-limiting step of that particular myosin. For example, smooth muscle myosin is highly regulated, and this mechanism seems to involve loop 2 (*16*). However, in unregulated myosins or myosins regulated in a different manner, loop 2 may still play an important role in actin activation but may use a different mechanism to achieve this activation, such as changes in K_m or relief of a suppressed activity. It should also be remembered that these studies have been carried out on purified actin and myosin. Other components, such as the tropomyosin/troponin system and myosin binding proteins, may interact in vivo with the loops as well. Therefore, the host myosin of the chimera may determine the mechanism and the extent to which the loop can affect the activity.

This work has shown that loop 2's location in the actin binding site allows it to modulate affinity for actin in response to signals from the rest of the molecule, enabling it to sense the nucleotide state and respond in the form of changes in actin affinity or conformation. In some systems, it may play a role in regulation as well (*16*). The proximity of loop 1 and loop 2 to the nucleotide and actin binding sites, coupled with the variability of their sequences, makes them ideal sites for affecting the rate-limiting steps of the actin−myosin ATPase cycle and force-generating steps. Myosin's two solvent-exposed, flexible loops provide the molecule with a mechanism for fine-tuning certain activities while maintaining the rest of the motor's activity, allowing each myosin isoform to carry out its specific role in the cell.

ACKNOWLEDGMENT

We thank Michael Geeves, the 1997 EMBO course on Pre-Steady-State Kinetics, and Stephan Schmitz for assistance with the stopped-flow pyrene actin K_d experiment. Additionally, we thank Kim Giese, Daniel Herschlag, Suzanne Admiraal, and members of the Spudich lab for helpful discussions and critical reading of the manuscript. S. Admiraal also contributed the ATPγS purification procedure.

REFERENCES

1. Chock, S. P., Chock, P. B., and Eisenberg, E. (1976) *Biochemistry 15*, 3244−53.
2. Lymn, R. W., and Taylor, E. W. (1971) *Biochemistry 10*, 4617−24.
3. Stein, L. A., Schwarz, R. P., Jr., Chock, P. B., and Eisenberg, E. (1979) *Biochemistry 18*, 3895−909.
4. Huxley, H. E. (1969) *Science 164*, 1356−66.
5. Goldman, Y. E. (1987) *Annu. Rev. Physiol. 49*, 637−54.
6. Geeves, M. A. (1991) *Biochem. J. 274*, 1−14.
7. Mornet, D., Pantel, P., Audemard, E., and Kassab, R. (1979) *Biochem. Biophys. Res. Commun. 89*, 925−32.
8. Rayment, I., Rypniewski, W. R., Schmidt-Base, K., Smith, R., Tomchick, D., Benning, M. M., Winkelmann, D. A., Wesenberg, G., and Holden, H. (1993) *Science 261*, 50−8.
9. Fisher, A. J., Smith, C. A., Thoden, J. B., Smith, R., Sutoh, K., Holden, H., and Rayment, I. (1995) *Biochemistry 34*, 8960−72.
10. Sellers, J. R., and Goodson, H. V. (1995) in *Motor proteins 2: Myosin* (Sheterline, P., Ed.) Vol. 2, pp 1323−423, Academic Press, London.
11. Goodson, H. V., Warrick, H., and Spudich, J. A. (1999) *J. Mol. Biol.* (in press).
12. Uyeda, T. Q.-P., Ruppel, K. M., and Spudich, J. A. (1994) *Nature 368*, 567−9.
13. Yamamoto, K. (1991) *J. Mol. Biol. 217*, 229−33.
14. Bertrand, R., Derancourt, J., and Kassab, R. (1989) *FEBS Lett. 246*, 171−6.
15. Spudich, J. A. (1994) *Nature 372*, 515−8.
16. Rovner, A. S., Freyzon, Y., and Trybus, K. M. (1995) *J. Biol. Chem. 270*, 30260−3.
17. Furch, M., Geeves, M., and Manstein, D. J. (1998) *Biochemistry 37*, 6317−26.
18. Ruppel, K. M., Uyeda, T. Q.-P., and Spudich, J. A. (1994) *J. Biol. Chem. 269*, 18773−80.
19. Manstein, D. J., Schuster, H.-P., Morandini, P., and Hunt, D. M. (1995) *Gene 162*, 129−34.
20. Manstein, D. J., and Hunt, D. M. (1995) *J. Muscle Res. Cell Motil. 16*, 325−32.
21. Giese, K. C., and Spudich, J. A. (1997) *Biochemistry 36*, 8465−73.
22. Pardee, J. D., and Spudich, J. A. (1982) *Methods Cell Biol. 24*, 270−89.
23. Criddle, A. H., Geeves, M. A., and Jeffries, T. (1985) *Biochem. J. 232*, 343−9.
24. McKillop, D. F. A., Fortune, N. S., Ranatunga, K. W., and Geeves, M. A. (1994) *J. Muscle Res. Cell Motil. 15*, 309−18.
25. Ritchie, M. D., Geeves, M. A., Woodward, S. K. A., and Manstein, D. J. (1993) *Proc. Natl. Acad. Sci. U.S.A. 90*, 8619−23.
26. Kurzawa, S. E., and Geeves, M. A. (1996) *J. Muscle Res. Cell Motil. 17*, 669−76.
27. Wagner, P. D. (1981) *J. Biol. Chem. 256*, 2493−8.

28. Fersht, A. (1985) in *Enzyme Structure and Mechanism*, 2nd ed., pp 105−6, W. H. Freeman and Co., New York.
29. Hermann, C., Wray, J., Travers, F., and Barman, T. (1992) *Biochemistry 31*, 12227−32.
30. Zhao, L., Naber, N., and Cooke, R. (1995) *Biophys. J. 68*, 1980−90.
31. Regnier, M., Morris, C., and Homsher, E. (1995) *Am. J. Physiol. 269*, c1532−9.
32. Murphy, C. T., and Spudich, J. A. (1998) *Biochemistry 37*, 6738−44.
33. Cook, R. K., Blake, W. T., and Rubenstein, P. A. (1992) *J. Biol. Chem. 267*, 9430−6.
34. Cook, K. R., Root, D., Miller, C., Reisler, E., and Rubenstein, P. A. (1993) *J. Biol. Chem. 268*, 2410−5.
35. Geeves, M. A., Goody, R. S., and Gutfreund, H. (1984) *J. Muscle Res. Cell Motil. 5*, 351−61.
36. Geeves, M. A., and Conibear, P. B. (1995) *Biophys. J. 68*, 194s−201s.
37. Geeves, M. A., and Jeffries, T. E. (1988) *Biochem. J. 256*, 41−6.
38. Shriver, J. W. (1986) *Biochem. Cell. Biol. 64*, 265−76.
39. Bobkov, A. A., Bobkova, E. A., Lin, S.-H., and Reisler, E. (1996) *Proc. Natl. Acad. Sci. U.S.A. 93*, 2285−9.
40. Umemoto, S., and Sellers, J. R. (1990) *J. Biol. Chem. 265*, 14864−9.
41. Siemankowski, R. F., Wiseman, M. O., and White, H. D. (1985) *Proc. Natl. Acad. Sci. U.S.A. 82*, 658−62.
42. Kurzawa-Goertz, S. E., Perreault-Micale, C. L., Trybus, K. M., Szent-György, A. G., and Geeves, M. A. (1998) *Biochemistry 37*, 7517−25.
43. Sweeney, H. L., Rosenfeld, S. S., Brown, F., Faust, L., Smith, J., Xing, J., Stein, L. A., and Sellers, J. R. (1998) *J. Biol. Chem. 273*, 6262−70.
44. Toyoshima, Y. Y., Kron, S. J., McNally, E. M., Niebling, K. R., Toyoshima, C., and Spudich, J. A. (1987) *Nature 328*, 536−9.
45. Bobkov, A., Sutoh, K., and Reisler, E. (1997) *J. Muscle Res. Cell Motil. 18*, 563−71.
46. Sellers, J. R., Eisenberg, E., and Adelstein, R. S. (1982) *J. Biol. Chem. 257*, 13880−3.

BI9826815